ADVANCED FUNCTIONAL MATERIALS
www.afm-journal.de

Controlling the Thermoelectric Properties of Organometallic Coordination Polymers via Ligand Design

*Zilu Liu, Tianjun Liu, Christopher N. Savory, José P. Jurado, Juan Sebastián Reparaz, Jianwei Li, Long Pan, Charl F. J. Faul, Ivan P. Parkin, Gopinathan Sankar, Satoru Matsuishi, Mariano Campoy-Quiles, David O. Scanlon, Martijn A. Zwijnenburg, Oliver Fenwick, and Bob C. Schroeder**

Organometallic coordination polymers (OMCPs) are a promising class of thermoelectric materials with high electrical conductivities and thermal resistivities. The design criteria for these materials, however, remain elusive and so far material modifications have been focused primarily on the nature of the metal cation to tune the thermoelectric properties. Herein, an alternative approach is described by synthesizing new organic ligands for OMCPs, allowing modulation of the thermoelectric properties of the novel OMCP materials over several orders of magnitude, as well as controlling the polarity of the Seebeck coefficient. Extensive material purification combined with spectroscopy experiments and calculations furthermore reveal the charge-neutral character of the polymer backbones. In the absence of counter-cations, the OMCP backbones are composed of air-stable, ligand-centered radicals. The findings open up new synthetic possibilities for OMCPs by removing structural constraints and putting significant emphasis on the molecular structure of the organic ligands in OMCP materials to tune their thermoelectric properties.

1. Introduction

Energy security is one of the cornerstones of economic and human prosperity. However, with the imminent threat of irreversible climate changes looming, caused by high levels of anthropogenic greenhouse gas emissions (e.g., carbon dioxide, methane), it is essential to realign the primary energy sources and to reduce the current dependence on fossil fuels (e.g., oil, coal, gas). While aiming for carbon neutrality should be the ultimate goal, the development of transition technologies to improve energy efficiency in the short term could have a profound and immediate impact on current carbon footprints. Presently around 60% (around 350×10^{18} J) of the global energy input is lost as waste heat after conversion; the equivalent of burning an additional 60×10^{9} barrels of oil per annum.[1] By recovering this wasted heat and converting it back into usable energy, i.e., electricity, the overall energy efficiency would be improved thereby reducing the demand for further fossil fuel combustion. One of the most promising technologies for waste heat recovery is thermoelectric generators (TEG), which convert a heat differential into an electrical potential, a phenomenon known as the Seebeck effect.[2] Most

Z. Liu, Dr. C. N. Savory, J. Li, Prof. I. P. Parkin, Prof. G. Sankar, Prof. D. O. Scanlon, Dr. M. A. Zwijnenburg, Dr. B. C. Schroeder
Department of Chemistry
University College London
London WC1H 0AJ, UK
E-mail: b.c.schroeder@ucl.ac.uk

T. Liu, Dr. O. Fenwick
School of Engineering and Materials Science
Queen Mary University of London
London E1 4NS, UK

Dr. C. N. Savory, Prof. D. O. Scanlon, Dr. M. A. Zwijnenburg
Thomas Young Centre
University College London
London WC1E 6BT, UK

The ORCID identification number(s) for the author(s) of this article can be found under https://doi.org/10.1002/adfm.202003106.

DOI: 10.1002/adfm.202003106

J. P. Jurado, Dr. J. S. Reparaz, Dr. M. Campoy-Quiles
Institut de Ciència de Materials de Barcelona-CSIC
Esfera UAB
Bellaterra 08193, Spain

Dr. L. Pan, Prof. C. F. J. Faul
School of Chemistry
University of Bristol
Bristol BS8 1TS, UK

Dr S. Matsuishi
Materials Research Center for Element Strategy
Tokyo Institute of Technology
Nagatsuta-cho, Midori-ku, Yokohama 226-8503, Japan

Prof. D. O. Scanlon
Diamond Light Source Ltd.
Diamond House
Harwell Science and Innovation Campus
Didcot, Oxfordshire OX11 0DE, UK

TEGs employed these days focus on the recovery of high-temperature waste heat (>500 °C) because the employed inorganic materials are expensive and therefore need to be operated at large temperature differentials to maximize device performance and economic return. However, over 50% of waste heat originates from low temperature sources (<200 °C), which so far cannot be recovered in an economically viable way. Organic TEGs on the other hand have the potential to bridge this gap because the thermoelectric materials are based on synthetic organic materials. The typically low elastic modulus of organic materials, compared to their inorganic counterparts, allows the fabrication of conformal TEG to harvest waste heat from complex shapes (e.g., hot water pipes, human body).[3]

To enhance the currently low thermal voltages obtained with organic materials, it is essential to develop new compounds, able to harvest low-temperature waste heat more efficiently.[4] The ideal thermoelectric material should simultaneously possess both a low electrical and high thermal resistivity in order to maximize the figure of merit zT. While conceptually simple, the synthesis of such materials has proven challenging to this day. One class of materials that have shown promising thermoelectric properties are organometallic coordination polymers (OMCPs). The ladder-type polymers, with the general formula poly[A_x(M-ett)], were first reported by Poleschner et al. for their excellent electrical properties.[5] Over the past years, OMCP materials, poly[Na_x(Ni-ett)] (where Ni-ett is nickel ethenetetrathiolate) in particular, have been intensely researched for their thermoelectric properties with zT values exceeding 0.3.[6] The insolubility of all OMCP materials however significantly hampers the fabrication of conformal TEGs. To improve their processability, OMCPs are routinely blended into a supporting polymer binder such as polyvinylidene fluoride or polyurethane. The composite films showed dramatically improved processability, however at the cost of reduced thermoelectric performance.[7] Alternatively, careful electrochemical synthesis allowed the deposition of poly[Na_x(Ni-ett)] onto flexible substrates, simultaneously enhancing the flexibility and thermoelectric performance of conformal TEG devices.[8] Despite the breadth of studies focusing on optimizing the synthesis, reproducibility, and processability of poly[A_x(M-ett)], the design of chemically distinct OMCPs has been neglected.

A comprehensive understanding of the structural and electronic properties of such insoluble low-dimensional coordination polymers is still a scientific challenge. Recently several theoretical works aimed at predicting the electrical and thermal characteristics of a series of π-conjugated transition-metal coordination polymers, but experimental studies on the effect of different organic ligands on the thermoelectric properties of the OMCPs have not been realized to date.[9] Herein, we present the synthesis of three different organic ligands and their incorporation into OMCPs with distinct thermoelectric properties. Notably, we experimentally demonstrate for the first time, that the n- or p-type thermoelectric character of the OMCP materials can be tuned via organic ligand modifications. Furthermore, we highlight the importance of adequate OMCP purification to study the intrinsic thermoelectric properties of the polymers, decoupled from any potential ionic impurities.

2. Results and Discussion

2.1. Synthesis

Poly(nickel-ethylenetetrathiolate) (Ni-ett) was prepared according to a previously published procedure from [1,3] dithiolo[4,5-*d*][1,3]dithiole-2,5-dione (**1**) (synthetic details provided in the Supporting Information), and the purification adapted (**Scheme 1**).[10] To increase the distance between the nickel centers, **1** was reductively dimerized in the presence of triethyl phosphite to yield [2,2′-bi[1,3]dithiolo[4,5-*d*][1,3]dithiolylidene]-5,5′-dione (**2**), which was polymerized to poly(nickel-[2,2′-bi(1,3-dithiolylidene)]-4,4′,5,5′-tetrakis(thiolate)) (Ni-diett) via formation of the tetra anion intermediate.[5] For the third OMCP, poly(nickel-benzene-1,2,4,5-tetrakis(thiolate) (Ni-btt), an aromatic ligand based on benzene-1,2,4,5-tetrathiol was introduced between the nickel centers. 1,2,4,5-tetrachlorobenzene (**3**) was reacted with propane-2-thiol via nucleophilic aromatic substitution (S_NAr) to yield 1,2,4,5-tetrakis(isopropylthio)benzene (**4**). Following dealkylation

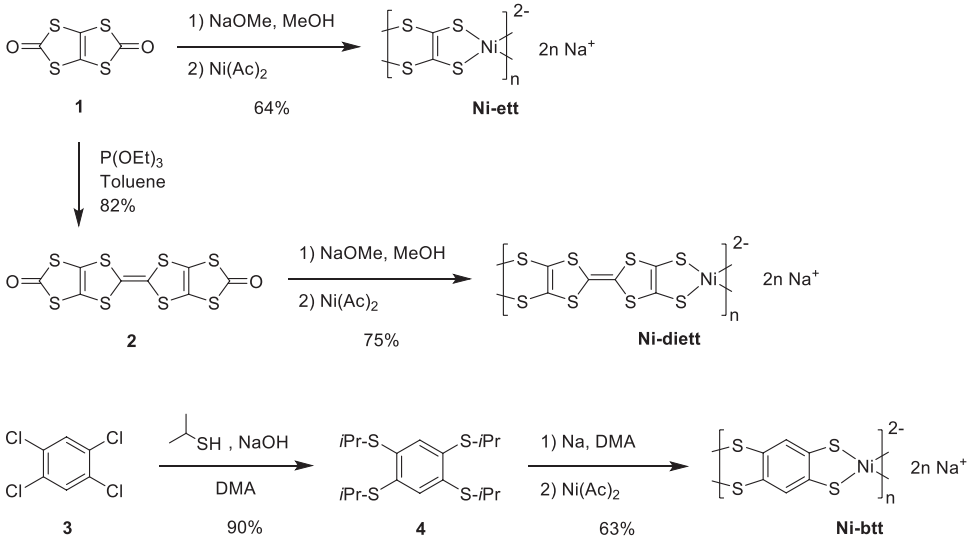

Scheme 1. Synthetic pathway toward the different OMCPs, Ni-ett, Ni-diett, and Ni-btt, and their idealized chemical structures with sodium counter cations.

with sodium, the resulting tetrathiolate was coordinated with nickel (II) acetate to form Ni-btt.

Although the reaction ratio of nickel acetate to organic ligand was 1:1, the insoluble nature of the OMCPs makes the inclusion of low molecular weight and ionic impurities in the material bulk likely. To avoid any adverse effects of impurities on the thermoelectric properties, the polymers were purified via Soxhlet extraction in deionized water (24 h), followed by methanol (24 h). The efficient removal of impurities from the OMCPs greatly enhanced the reproducibility of their physical properties and dramatically reduced the batch-to-batch variations, a common problem in the synthesis of OMCP materials. The three polymers should possess a negatively charged framework in which the negative charge of each repeat unit is compensated by two monovalent cations, leading to an overall charge-balanced structure $[\text{M-ligand}]_n^{2-} \times 2n\ A^+$. However, in the case of the well-studied Poly[A_x(M-ett)], the equivalents of metal cations A (Li^+, Na^+, or K^+), acting as counter cations, were never found in sufficient quantities to even approximately balance the charge of the polymer backbone (M to alkali metal ratios of 3–100, Table S1, Supporting Information). One proposed interpretation is that M partially acts as counter cations, rather than purely central coordination metal based on X-ray photoelectron spectroscopy (XPS) analysis, while other researchers put forward a neutral polymer structure, known as poly(Ni-tetrathiooxalate) (Ni-tto).[11] To obtain a more detailed picture of the polymers' chemical composition and the effects of purification, a series of spectroscopic measurements was performed.

2.2. Compositional and Structural Characterization

As the three synthesized OMCPs were insoluble, we probed the sample morphology by scanning electron microscopy (SEM) and the composition by energy-dispersive X-ray spectroscopy (EDS). SEM images of the OMCPs confirmed an inhomogeneous particle size distribution, with the largest particles exceeding 100 µm, which subsequently would lead to rough, nonuniform samples and significant batch-to-batch variations (Figure S1, Supporting Information). The particle size was therefore mechanically decreased to 1–10 µm by ball milling. The smaller particle sizes lead to more homogenous samples when the OMCPs were compressed into pellets at 2.6 GPa, as evidenced by the smooth surfaces with minor cracks and imperfections. EDS mapping confirmed the compositional homogeneity of Ni-ett, Ni-diett, and Ni-btt pellets (Figure S2–S4, Supporting Information) and the corresponding elemental composition (**Table 1**). Due to the extensive Soxhlet purification, we believe it is unlikely that excess nickel in the OMCPs would cause the experimentally observed deviations in the S/Ni ratios, but rather structural defects along the polymer backbone. The experimental S/Ni ratios were closest to the theoretical values in Ni-diett and Ni-btt; we believe these results are related to the larger size of the organic ligand, facilitating the stabilization of the tetra thiolate intermediate during the OMCP synthesis leading to higher quality polymers. In the case of the Ni-ett synthesis, the stabilization of the charged intermediate is more difficult, leading to a richer chemistry and possibly the formation of various defects and isomers, ultimately resulting in a nonideal S/Ni ratio.[11,12]

Table 1. Elemental atomic percentages of C, S, and Ni in compressed polymer pellets based obtained by EDS analysis.

Sample	C	S	Ni	S/Ni ratio[a)]
Ni-ett	41.4	32.2	11.7	2.6 (4)
Ni-diett	51.2	37.5	5.7	6.6 (8)
Ni-btt	66.0	20.7	6.0	3.5 (4)

[a)]Theoretical values are given in parentheses.

XPS was employed to investigate the composition of Ni-ett, Ni-diett, and Ni-btt. XPS energy survey scans on the pristine, nonpurified polymers showed the presence of Ni 2p, C 1s, S 2p, and Na 1s core levels (Figure S5–S7, Supporting Information). In earlier studies, the Na 1s signal in the XPS energy survey spectra was assigned to Na^+ counter ions.[6a,7c] However, after purifying the OMCPs through extensive Soxhlet extractions, the Na 1s peak initially located at a binding energy of 1071 eV completely disappeared. X-ray fluorescence (XRF) results (Table S2, Supporting Information) also confirmed the absence of Na in Ni-ett, Ni-diett, and Ni-btt. Furthermore, the C 1s peak centered around 289 eV, and associated with carbonyl functional groups, was no longer detectable in the purified samples. The successful removal of any carbonate and acetate salts formed during the polymer synthesis and the efficacy of Soxhlet extraction to purify the OMCP polymers was thus confirmed.

In the Ni 2p photoemission spectra of the purified OMCPs, the set of peaks with binding energies of 853 and 873 eV, were assigned to the Ni $2p_{3/2}$ and Ni $2p_{1/2}$, confirming the presence of Ni^{2+} species. In case of pristine Ni-ett, two distinct Ni $2p_{3/2}$ peaks, derived from XPS fitting at 855.8 and 853.4 eV, were observed, implying the coexistence of two nickel environments, either in a square planar coordination complex or as counter cation. Some reports attributed a similar Ni $2p_{3/2}$ spectra to a single type of centered Ni atom in a 2D organic framework.[6a,13] However, by comparing the Ni $2p_{3/2}$ peaks of as-prepared and purified Ni-ett, there was an evident decrease of the fitted peak at 855.8 eV and a disappearance of the satellite signal around 861 eV in the purified Ni-ett. As neither EDS nor XRF measurements confirmed the existence of nickel impurities in the sample, we believe the two Ni $2p_{3/2}$ signals originated from multiplet-splitting, which is commonly observed in inorganic nickel compounds, such as NiO, $Ni(OH)_2$, and NiS, rather than different nickel environments.[14]

The S 2p narrow range scans of the three purified polymers all showed main peaks with binding energies of 161.9 and 163.3 eV, deriving from the complexation between Ni and S units (Figure S5–S7, Supporting Information). Prior to purification, the S 2p spectra of both Ni-ett and Ni-diett also presented a weak peak at 168.3 eV, which is ascribed to sulfate moieties, consistent with reported values.[15] Further evidence to corroborate the partial sulfur oxidation was found in the S 2p XPS spectra of Ni-ett samples exposed to air over a period of 12–18 months (Figure S8 and S9, Supporting Information). After 12-month ambient storage, a very intense peak, centered around 168.5 eV, emerged in the Ni-ett sample, becoming significantly more pronounced after 18 months of air exposure, surpassing the Ni—S peak. The oxidation was not limited to surface oxidation, as evidenced by the depth profiling

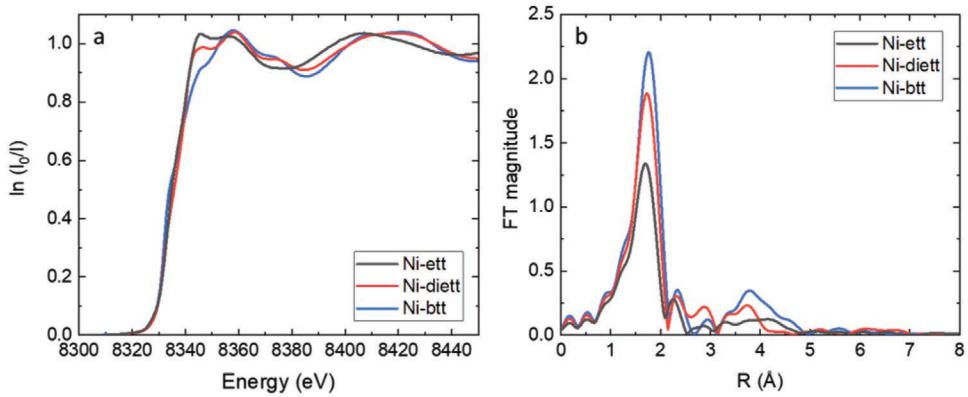

Figure 1. Ni K-edge XANES spectra of Ni-ett, Ni-diett, and Ni-btt a) and the Fourier transform magnitudes of the Ni K-edge EXAFS b).

(Figure S10, Supporting Information) and the recurring presence of the sulfite peak around 168.5 eV. Notably, purification via Soxhlet extraction was able to remove the oxidized impurities as evidenced by the significant reduction of the S 2p signal originating from sulfite groups (Figure S9, Supporting Information). As the purification is not performed under reductive conditions, we hypothesize that the formation of soluble sulfite impurities is accompanied by partial depolymerization during the oxidation process.

Nickel k-edge X-ray absorption near-edge structure (XANES) measurements were performed to gain more detailed insights into the geometry of the Ni−S complexes within the OMCPs. The data and corresponding spectra are shown in **Figure 1**, and summarized in Table S3, Supporting Information. The position of the absorption edge is similar in all three samples, implying identical oxidation states for the Ni. However, significant differences at the top of the edge between 8340 and 8370 eV, hint toward structural variations in the Ni−S environments. The Fourier transforms shown in Figure 1b highlight the differences in magnitude of the first peak representing Ni−S distances. The differences are attributed to an increase in structural disorder, with the lowest degree of disorder in the Ni−S environment observed for Ni-diett, and the highest for Ni-ett. It is difficult to trace the origins of the increased disorder, yet they could be understood in terms of the more extensive resonance structures in Ni-ett and Ni-btt, which consequently lead to larger variations in Ni−S bond lengths, compared with Ni-diett its more limited resonance structure.

As all three materials, Ni-ett, Ni-diett, and Ni-btt, contain thioether bonds and organic ligands with differing electron-donating character, a combination of attenuated total reflection Fourier transform infrared (FTIR) and resonance Raman spectroscopies was explored to characterize the three Ni^{2+}-thiolate coordinated polymers in more detail and to obtain insight into the nature of the Ni−S bonding (**Figure 2**). The corresponding spectra of compounds (**1**, **2**, and **4**) were recorded and can be found in Figure S11 and S13, Supporting Information.

Previous reports focused on a series of square planar complexes formed with Ni^{II} and methyl or butyl substituted benzene-1,2-dithiolate, namely $(L^{Me})^{2-}$ or $(L^{Bu})^{2-}$. The monoanionic structure $[Ni^{II}(L^{alkyl})(L^{alkyl\cdot})]^{-}$ was found to be remarkably stable under ambient conditions, and like the neutral diamagnetic compound $[Ni^{II}(L^{alkyl\cdot})_2]^0$ possessed a π-radical-anion character.[16] More recently, the presence of the C = S˙ stretching vibration mode (1114–1082 cm^{-1} in) spectra) revealed the presence of S,S-coordinated radicals in organometallic complexes based on 3,5-ditertbutyl-benzene-1,2-dithiolato ligands and divalent metal centers (Ni, Pd, Pt).[17] Extending these findings to Ni-ett, C = S˙ stretching vibration modes are observed at 1163 and 1074 cm^{-1} in the IR spectrum. Similar bands can be found for Ni-diett with a split peak located at 1173–1142 cm^{-1} and a weaker peak at 1038 cm^{-1}. This is in stark contrast to the IR absorption bands of υ(C = S), which manifest as strong

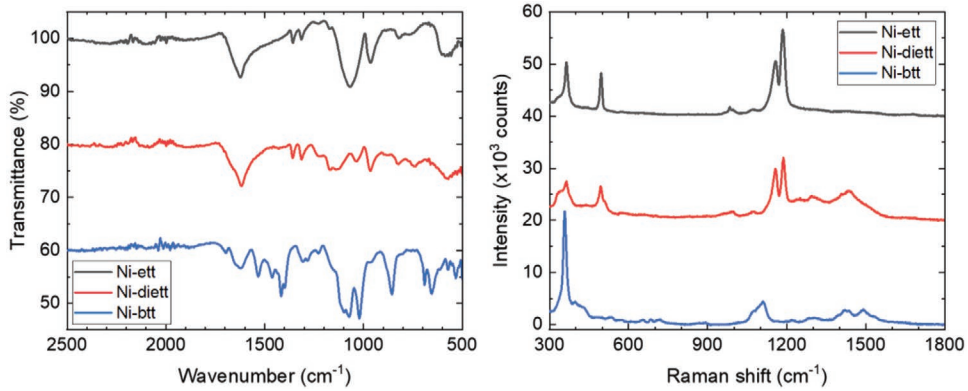

Figure 2. FTIR a) and resonance Raman b) spectra of the three OMCPs after purification. The spectra have been stacked for clarity.

bands (no split peak) at wavenumbers around 1146 cm^{-1}, as previously demonstrated in Ni^{2+} complexes.[18] The results from the IR-spectra are corroborated by Raman spectroscopy. Both Raman spectra of Ni-ett and Ni-diett present similar split peaks at 1158 and 1186 cm^{-1}, confirming the presence of thiocarbonyl radicals (C = S·). Furthermore, both polymers show equivalent peaks at 364 and 496 cm^{-1}, representing the υ(Ni—S) and ring deformation, respectively.[19] The overall high similarity at lower wavenumbers (<1200 cm^{-1}) between the two Raman spectra can be explained by the intrinsic similarity of Ni-ett and Ni-diett in terms of the organic ligands and chemical bonds. However, at larger wavenumbers (>1200 cm^{-1}) the Ni-diett spectrum resembles the Ni-btt spectrum and both spectra show a series of weaker peaks at 1297, 1430, and 1491 cm^{-1}, features absent in the Ni-ett spectrum. In Ni-btt, these signals are assigned to the H—C—C scissoring vibration, the aromatic semicircular stretching, and the ring quadrant stretching mode, respectively, which correspondingly are also observed in the Raman spectra of compound 4 (Figure S13, Supporting Information).[20] In case of Ni-diett, due to the absence of an aromatic ring and by comparison to the spectrum of **2**, the peaks are assigned to the remaining inner-ring and ring-bridging C = C stretch vibration, supported by the presence of sharp peaks at 1474 and 1495 cm^{-1}.

Analogously, the broad peak around at 1100 cm^{-1} found in the Raman spectrum of Ni-btt is assigned to the (Ar)C = S stretching vibration in the ligand. Correspondingly, the IR spectrum of Ni-btt shows a split peak around 1100 cm^{-1} and a strong peak at 1019 cm^{-1}, in line with the abovementioned υ(C = S·) bands involving radical anion ligands. The intense peak at 357 cm^{-1} results from the Ni—S stretching vibrations. Taking into account all spectroscopic data, as well as the elemental composition obtained by EDS and XRF, it becomes clear that the synthesized OMCP materials do not contain a significant number of counter cations, leading to the conclusion that the organometallic backbone does not possess an overall net charge. This interpretation is further substantiated by the combined IR and Raman studies, confirming the presence of thiocarbonyl radicals (C = S·) in all OMCPs and supporting the radical structures proposed in **Scheme 2**.

Powder X-ray diffraction was performed to investigate the solid-state order of the different OMCP materials, and the diffraction patterns are shown in Figure S14, Supporting Information. Both Ni-ett and Ni-diett presented a broad diffraction peak at 11.9°, corresponding to a lamellar stacking distance of 3.42 Å. Given the structural similarity between Ni-ett and Ni-diett, it is not surprising both materials present identical d-spacings. The diffraction pattern for Ni-btt on the other hand showed two diffraction peaks, an intense peak at 6.0° and a weaker, much broader, and split peak around 11.9°. The bulkier, six-membered benzene ring in Ni-btt lead to a larger d-spacing of 6.78 Å compared with Ni-ett and Ni-diett. While the diffraction peaks are weak in overall intensity, they confirm that the synthesized OMCP materials are not amorphous and that the ligand structure has a profound impact on the molecular packing, especially on the lamellar stacking distances.

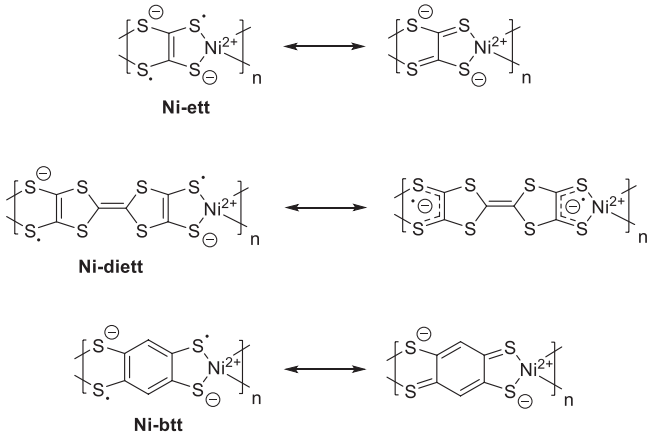

Scheme 2. Proposed chemical structures of charge neutral OMCPs.

2.3. Electronic Structure Characterization

Ultraviolet photoelectron spectroscopy was performed to determine the work functions and densities of valence electronic states (Figure S15, Supporting Information). The lowest work function (Φ) was measured for Ni-btt (4.9 eV), whereas the work functions for Ni-ett (4.7 eV) and Ni-diett (4.6 eV) were similar, given the structural similarity between both compounds. Closer to the Fermi energy (E_F) level, the three OMCPs present disorder-induced tails extending toward the E_F, rather than sharp edges. Similar, behavior was previously reported for poly(3,4-ethylenedioxythiophene):poly-styrene sulfonate, and the tail associated with localized filled states induced by disorder within the polymer structure.[21]

The temperature dependence of the OMCP's magnetization (*M*) was measured by a superconducting quantum interference device (SQUID), which is shown in **Figure 3**. Both Ni-ett and Ni-btt show typical antiferromagnetic behavior with small magnetic moments and peaks around 8 K in the zero-field cooling in their respective *M-T* curves. However, the peaks are absent in the field cooling (FC) *M-T* curves, indicating that the weak spontaneous magnetization is induced by the applied magnetic field. This hypothesis is further supported by the hysteresis loops observed in the *M-H* curves at 2 K. Despite the high magnetic fields (up to 50 kOe), the magnetization did not saturate, implying that it is instigated by spin canting in antiferromagnetic states. Ni-ett showed an order of magnitude larger magnetization than Ni-btt regardless of the similarities between their *M-T* and *M-H* curves. The magnetization for Ni-diett is significantly smaller and the FC curve obeys the simple Curie-Weiss law ($\chi_m = C_m/(T\text{-}\theta)$), in contrast to Ni-ett and Ni-btt, whose FC curves follow the Curie-Weiss equation, $\chi_m = C_m/(T - T_c)$ down to the critical temperature (T_c). All extracted parameters such as Curie constant (C_m) and Weiss temperature (θ) are provided in Figure S16–S18, Supporting Information.

The electronic structure of the OMCP materials was further investigated by electron paramagnetic resonance (EPR) spectroscopy. All three samples showed weak EPR signals, with the signal for Ni-ett being significantly different, both in signal strength and shape, to Ni-diett and Ni-btt measurements (Figure 5). The broad signal observed for Ni-ett around 100 mT could be attributed to biradical with an integer spin state (S = 1 and g ~ 2), and the zero-field splitting parameter (b_2^0) ~ 0.314 cm^{-1}

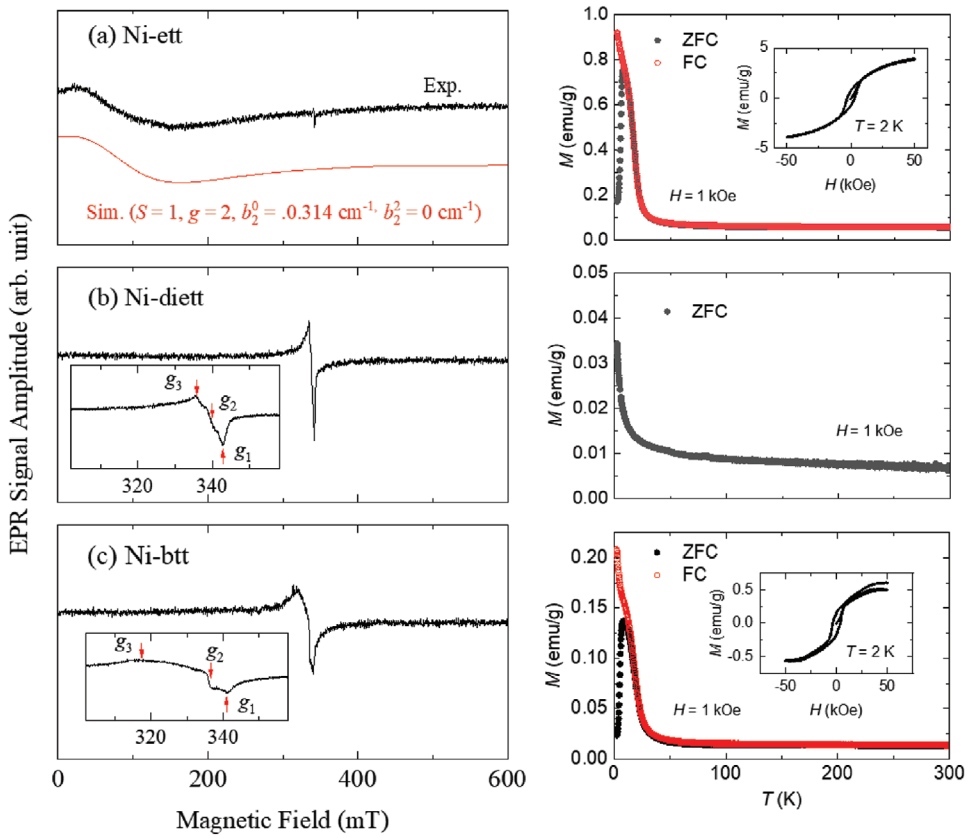

Figure 3. (Left column) First-derivative EPR spectra of Ni-ett, Ni-diett and Ni-btt samples recorded at 77 K. (Right column) The corresponding SQUID measurements with *M-H* hysteresis curve measured at 2 K (inset). The simulated EPR pattern for Ni-ett was calculated with EasySpin software.[22]

is comparable to reported values for Ni^{2+} cations in inorganic hosts (Table S4, Supporting Information).[23] The exact origin of the extremely weak EPR signal for Ni-diett and Ni-btt samples is unknown, but could possibly originate from Ni^{3+} impurities with a half-integer spin (S = ½), in addition to Ni^{2+}.[24] It is noteworthy that while the XPS data did not specifically confirm the presence of Ni^{3+} in the OMCP samples, neither does it contradict the EPR findings as the Ni^{3+} XPS signal would be included in the Ni $2p_{3/2}$ centered around 855 eV and as such difficult to unambiguously deconvolute from the Ni^{2+} peak. Another possibility for the weak EPR signature could be the localization of unpaired electrons on the polymer end-groups, or defective chain ends. The spin concentration of unpaired electrons in the OMCPs was estimated by comparing the areal intensity of the EPR spectra, assuming an electron spin of S = ½ (Table S4, Supporting Information). All OMCP's show large spin concentrations between 1020 and 1022 spin per mole (around one per hundredth repeat unit), comparable to highly conducting polyaniline.[25] The magnetic moments per repeat unit calculated from the EPR signal however are smaller than the ones obtained from the SQUID measurements, indicating that the OMCP materials are mostly EPR silent, and the small signals observed are likely originating from EPR active impurities or chain defects.

Density functional theory (DFT) calculations on the free ett^{2-}, $diett^{2-}$, and btt^{2-} ligands suggest that in the case of diett the oxidation of the ligand from −4 to −2 results in the formation of an open-shell biradical (Table S5, Supporting Information). The dianions of the other two ligands are predicted to remain closed-shell. In all cases, oxidation of the ligands is accompanied by a symmetric reduction in the bond-lengths of the terminal C−S bonds by 0.1–0.2 Å. DFT calculations on ligand-terminated oligomeric models of chains consisting of five ligands and four nickel atoms, carrying a net charge of −2 or 0, when the terminal sulfur atoms of the capping ligands are replaced with hydrogen atoms (e.g., 1,2-ethenedithiol in the case of ett) as proxies for the case where the terminal sulfur atoms are oxidized to sulfonic acids or disulfides, as models of the polymers find complex electronic behavior (Tables S6–S10, Supporting Information). The ground state of the Ni-ett dianionic oligomer is predicted to be a closed-shell singlet, whereas that for the Ni-diett dianionic oligomer is an open-shell singlet with the majority of the unpaired spin density on the ligands. For the Ni-btt dianionic oligomer, the predicted ground state is an open-shell singlet with the majority of the unpaired spin density distributed over the four nickel atoms and the four terminal sulfur atoms. It is unclear if the latter polarized electronic solution is an artifact of our computational model or would occur experimentally. Regardless, we were for the dianionic Ni-btt oligomer, just as for the dianionic Ni-ett oligomer, unable to find the equivalent of the open-shell singlet state observed in the case of the Ni-diett dianion. In the case of the neutral oligomers capped with hydrogen terminated ligands, we find that for all three ligands the ground state is an open-shell singlet but that generally the triplet state lies very close in

energy, and that just as for the dianionic oligomers the majority of the spin is localized on the ligands. In the case of the neutral Ni-ett oligomer, the spin localizes near the end of the chain, for the neutral Ni-btt oligomer on the center of the oligomer, while in the case of neutral Ni-diett oligomer the spin is delocalized over the whole chain. The localization of the majority of the spin on the ligands rather the nickel observed in the DFT calculations on the dianionic and neutral oligomers, as well as for the periodic version of Ni-diett discussed below, is in line with the evidence for Ni^{2+} rather than Ni^{4+} from XPS and previous computational and experimental work.[17,26] Finally, the oligomeric models for each of the ligands, dianionic or neutral, were predicted to have absorption onset values in the near IR ($\lambda_{onset} > 1000$ nm).

The electronic structure of Ni-diett was further investigated by performing periodic DFT calculations on a unit cell of Ni-diett, comprising one monomer surrounded by 30 Å of vacuum in the two nonchain directions, to avoid interactions between chains. Multiple initial spin states were trialed, including initial magnetic moments on both the nickel atom and the ligand with both HSE06 and PBE0 functionals. An open-shell singlet state with spin density distributed across the ligand but a net zero magnetization was found to be the ground state, supporting the observations in the oligomeric simulations.

The electronic band structure and density of states of Ni-diett, calculated with HSE06, are included in Figure S19, Supporting Information. Overall the material has a narrow band gap of less than 0.5 eV with both valence and conduction bands primarily composed of the conjugated S 3p and C 2p states, with only minor contribution from the Ni atom. The band structure demonstrates the strong dispersion in the direction of the polymeric chain (Γ to X) and minimal dispersion in other directions consistent with the vacuum separation. Assuming a parabolic band, fitting to the band energies gives an electron effective mass of 0.176 m_0, which is low and consistent with the possibility for high mobility.

2.4. Thermoelectric Characterization

The three OMCP materials were synthesized as black brittle solids, making their processability challenging. As we were interested in the intrinsic thermoelectric properties, we refrained from blending the OMCPs with more processable binder polymers to eliminate any effects of the binder polymer itself, the composite morphology, and processing conditions on the thermoelectric properties of the OMCPs. To characterize the thermoelectric properties, powders of three OMCP materials were compressed into freestanding pellets (detailed fabrication conditions are outlined in the Supporting Information). All three OMCPs showed temperature-activated charge transport (**Figure 4**), with the highest electrical conductivity measured at room temperature (293 K) for Ni-ett (~10 S cm^{-1}) and the lowest for Ni-diett (~2 S cm^{-1}). While the thermal annealing at 150 °C for 5 h only had a minimal effect on the electrical conductivities, it had a much more profound impact on the Seebeck coefficients, particularly in the case of Ni-ett for which the Seebeck coefficient increased in magnitude from −26 μV K^{-1} to −86 μV K^{-1} after thermal annealing. The exact origin of this significant change in Seebeck coefficient is still under investigation. Extensive annealing could plausibly have allowed for the removal of volatile impurities from the OMCP pellet, which is in agreement with the thermal gravimetric measurements recording a slight weight loss (<3%) before thermal decomposition at around 300 °C, and 250 °C in the case of Ni-ett (Figure S20, Supporting Information). For Ni-diett the effects of the annealing were less pronounced, and the magnitude of the Seebeck coefficients increased slightly from −26 to −40 μV K^{-1} (at 305 K), respectively remained unchanged for Ni-btt.

The most striking difference however was that the Ni-btt showed a positive Seebeck coefficient of around 15 μV K^{-1} in the measured temperature range, contrary to Ni-ett and Ni-diett which demonstrated n-type characteristics. Previously, the charge polarity of poly(M-ett) materials was reported to be reliant on the nature of the central metal cation, making Ni-btt the first example to demonstrate that the carrier characteristics can be controlled via the organic ligand.[6a] Beyond the promising Seebeck coefficient, Ni-btt showed good electrical conductivities of 5 S cm^{-1} in pristine and 7 S cm^{-1} in annealed pellets at 293 K. It is noteworthy that this value is five orders of magnitude higher than the reported Ni-btt film prepared from benzene-1,2,4,5-tetrathiol via interfacial reaction.[27] This improvement is most likely due to the alternative synthetic route used here, where Ni^{2+} was directly reacted with the benzene-1,2,4,5-tetrathiolate to form the Ni-btt polymer in a strongly basic environment, limiting the possibility of oxidation of thiols to disulfides within the polymer chain.

The thermal conductivity was measured by Raman thermometry, using a single laser as a heater and a thermometer simultaneously, where the latter is conceptually based on the temperature-dependent spectral position of selected Raman modes.[28] In practice, the OMCP samples absorb the incident laser energy, which typically causes a thermal bathochromic shift in the Raman peak positions, as shown in **Figure 5**. Full experimental details are provided in the Supporting Information.

All three OMCP materials show low thermal conductivities (<2 W m^{-1} K^{-1}) in freestanding pellets, with the lowest value recorded for Ni-btt (1.2 W m^{-1} K^{-1}) and slightly increasing for Ni-diett (1.5 W m^{-1} K^{-1}) and Ni-ett (1.7 W m^{-1} K^{-1}) (**Table 2**). These values are higher than those previously reported for similar OMCP materials, which we attribute to the higher sample purity.[6a] To exclude that the differences in thermal conductivities observed for the three OMCP materials originate from inhomogeneities in the surface of the samples (e.g., roughness, composition, impurities), rather than from the differences in molecular structure, Raman imaging under high power (1 mW) laser illumination was performed (Figure S21, Supporting Information). While the surface topography of all three samples appeared inhomogeneous, Raman analysis provided further insight into the chemical composition. Both Ni-ett and Ni-diett samples presented a uniform chemical composition, yet with minor differences in the surface structure. The surface of Ni-ett exhibited smoother (red) and rougher domains (blue). After performing a cluster analysis on the Raman data, it became apparent however that the only difference between the two domains was a higher Raman intensity in the smoother regions. Similarly, Ni-diett presented a porous-like structure on

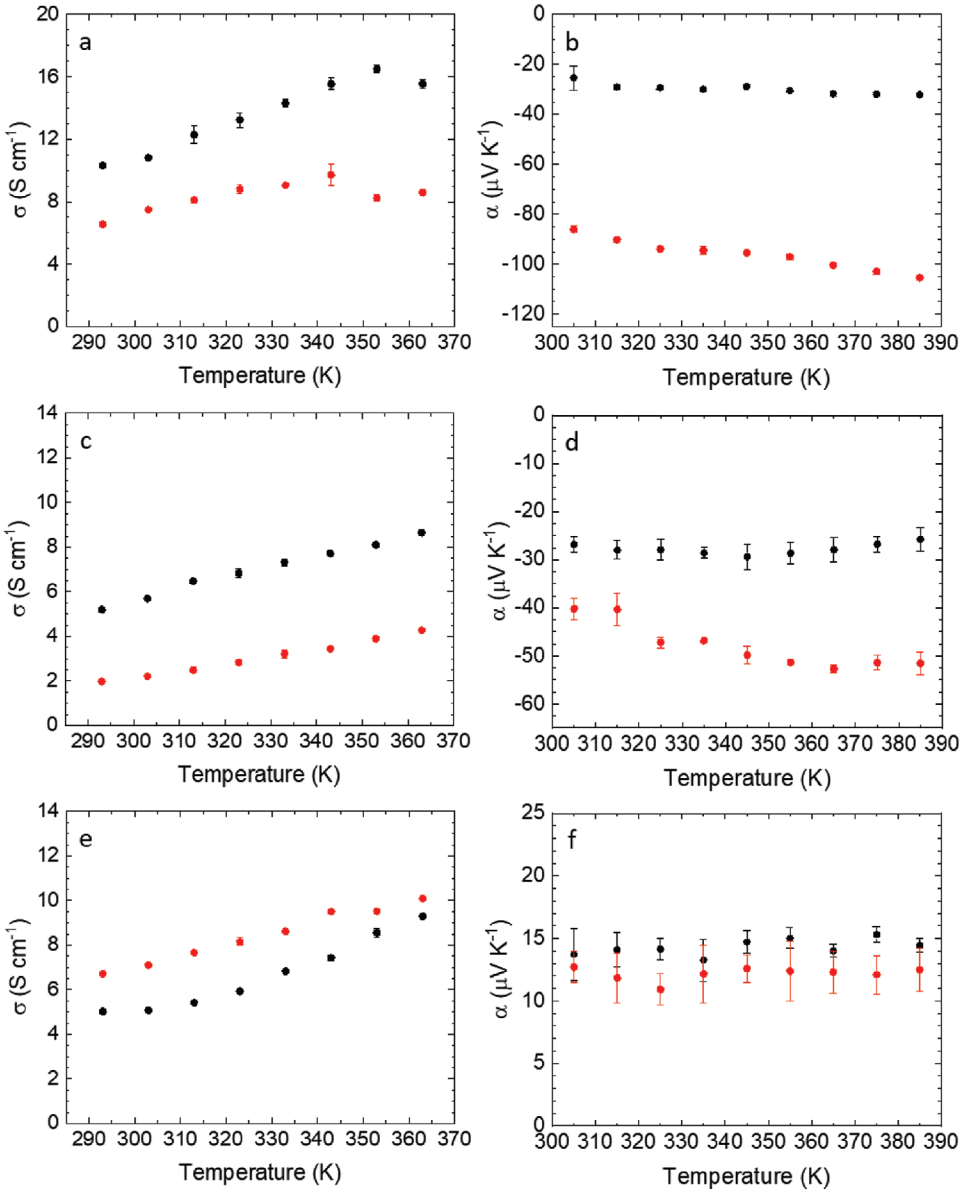

Figure 4. Electrical conductivities (left column) and Seebeck coefficients (right column) of Ni-ett a,b), Ni-diett c,d), and Ni-btt e,f) as a function of temperature. Data points obtained from pristine pellets (black) and from pellets annealed at 150 °C for 5 h in air (red).

the surface, with two distinct Raman spectra associated to the porous "holes" (blue) and the surrounding "scaffolding" (red), respectively. Ni-btt on the other hand revealed a much more complex picture. Not only was the surface rougher, but also its composition appeared to be inhomogeneous. The cluster analysis revealed three different Raman spectra. One identified as noise (purple), and the other two identified as distinct Raman signals (green and orange). The small differences in peak position and shape hint at modestly different chemical compositions and could account for the larger standard deviation recorded for the thermal conductivity of Ni-btt. In an attempt to gain additional information on the surface composition, we extended the spectral range of the Raman scans (Figure S22, Supporting Information). The bands between 300 and 500 cm^{-1} are associated with vibrations involving heavy atoms (the metal centers), while the broad band in the 1200–1600 cm^{-1} is associated with carbon bonds (the organic ligands). The fact that this peak is broad indicates the presence of amorphous carbon, or carbon with very different environments. The change in the ratio between the intensities of the inorganic and organic vibrations on the other hand suggests variations in stoichiometry among the different regions, which may be the reason why the thermal conductivity varies slightly from point to point. To quantify the potential differences in thermal conductivity, the spectra were fitted at the peak around 360 cm^{-1} and the histogram for each sample calculated (Figure S23 Supporting Information). The distribution of the spectral position of the Raman peak was relatively narrow in the case of Ni-ett (with most of the data lying within ± 5 cm^{-1}), while the distribution was much broader for Ni-ett and Ni-btt (about ± 25 cm^{-1}). These deviations

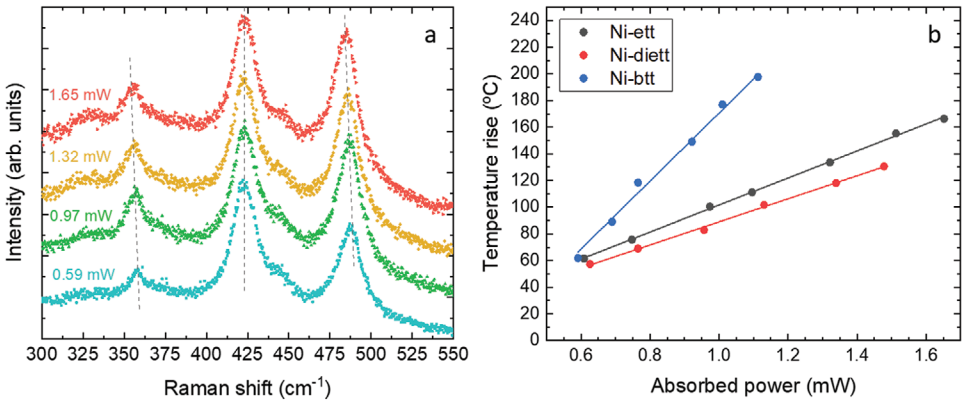

Figure 5. a) Representative Raman spectra at different absorbed powers for Ni-diett. Note that the peaks around 360 cm^{-1} and 490 cm^{-1} exhibit the largest bathochromic shift as the absorbed power increases. b) Calibrated temperature rise of each OMCP sample as a function of the absorbed power.

are entirely consistent with the increase in the standard deviation observed from the three different positions at which the Raman thermometry experiments were performed. In light of the detailed surface characterization and careful statistical analysis, the differences in thermal conductivity observed for the three OMCP materials are most likely originating from the different chemical structures, rather than being related to experimental errors.

3. Conclusion

Novel OMCPs were successfully synthesized by developing and optimizing the bulk synthetic procedure and putting significant emphasis on the material purification. Extensive spectroscopic analysis confirmed the molecular structure and composition of the new materials (Ni-diett and Ni-btt) and highlighted the importance of adequate OMCP purification. DFT calculations, supported by EPR and SQUID experiments, further revealed the open-shell character of the Ni-diett with the unpaired spin primarily localized on the organic ligand, rather than on the metal complex. The materials showed promising thermoelectric properties at room temperature, and possibility to tune the charge carrier polarity via the modification of the organic ligands in OMCP materials, rather than relying solely on the nature of the metallic cation, which was demonstrated for the first time. This finding opens up new synthetic possibilities and renders the design of new, better performing OMCPs more versatile, by removing structural constraints and putting significant emphasis on the molecular structure of the organic ligands in OMCP materials to tune their thermoelectric properties.

Table 2. Summary of the average thermoelectric properties at 305 K of annealed OMCPs.

Sample	σ [S cm^{-1}]	α [μV K^{-1}]	κ [W m^{-1} K^{-1}]	Power factor [μW m^{-1} K^{-2}]	zT
Ni-ett	7.49 ± 0.05	−86.1 ± 1.2	1.7 ± 0.2	5.55 ± 0.19	1×10^{-3}
Ni-diett	5.70 ± 0.05	−40.2 ± 1.6	1.5 ± 0.4	0.94 ± 0.08	2×10^{-4}
Ni-btt	7.11 ± 0.01	12.7 ± 1.2	1.2 ± 0.5	0.12 ± 0.02	3×10^{-5}

Supporting Information

Supporting Information is available from the Wiley Online Library or from the author.

Acknowledgements

The authors gratefully acknowledge Dr. Mark Baxendale for the use of the MMR Seebeck instrument, as well as Dr. Shibo Xi for the support and assistance provided during the XANES measurements. Z.L., T.L. and J.L. acknowledge the support from Chinese Scholarship Council (CSC). B.C.S. acknowledges funding by the Leverhulme Trust (Grant RF-2017-655\4) and the EPSRC (EP/P007767/1). M.A.Z. acknowledges the UK Engineering and Physical Sciences Research Council (EPSRC) for funding (Grant EP/N004884/1, Integration of Computation and Experiment for Accelerated Materials Discovery). B.C.S. and M.A.Z. acknowledge the EPSRC (Grant EP/R034540/1, Defect Functionalized Sustainable Energy Materials: From Design to Devices Application). O.F. acknowledges the support of The Royal Society (UF140372). The authors at ICMAB would like to acknowledge financial support from the Spanish Ministry of Science, Innovation and Universities through the "'Severo Ochoa"' Program for Centers of Excellence in R&D (SEV-2015-0496), PGC2018-095411-B-I00, and MAT2017- 90024-P, and from the European Research Council (ERC) under grant agreement no. 648901. J. P. J. has received financial support through the "la Caixa" INPhINIT Fellowship Grant (Grant code: LCF/BQ/IN17/11620035). L.P. acknowledges a Newton Fellowship from the Royal Society for funding (grant reference NF170361). The use of the UCL Legion, Myriad, and Grace High Performance Computing Facilities (Legion@UCL, Myriad@UCL and Grace@UCL) is acknowledged in the production of this work. Computational work was also performed on the ARCHER UK National Supercomputing Service, via our membership of the UK's HEC Materials Chemistry Consortium, funded by EPSRC (EP/L000202 and EP/R029431), and the UK Materials and Molecular Modelling Hub, which is partially funded by EPSRC (EP/P020194/1).

Conflict of Interest

The authors declare no conflict of interest.

Keywords

coordination polymer, hybrid thermoelectric materials, organometallic chemistry, Seebeck coefficient, thermal conductivity

Received: April 7, 2020
Revised: May 9, 2020
Published online:

[1] a) C. Forman, I. K. Muritala, R. Pardemann, B. Meyer, *Renewable Sustainable Energy Rev.* **2016**, *57*, 1568; b) *BP Statistical Review of World Energy 2019*, BP Amoco, London **2019**.
[2] G. J. Snyder, E. S. Toberer, *Nat. Mater.* **2008**, *7*, 105.
[3] a) L. M. Cowen, J. Atoyo, M. J. Carnie, D. Baran, B. C. Schroeder, *ECS J. Solid State Sci. Technol.* **2017**, *6*, N3080; b) H. Fang, B. C. Popere, E. M. Thomas, C.-K. Mai, W. B. Chang, G. C. Bazan, M. L. Chabinyc, R. A. Segalman, *J. Appl. Polym. Sci.* **2017**, *134*.
[4] a) P. J. Taroni, I. Hoces, N. Stingelin, M. Heeney, E. Bilotti, *Isr. J. Chem.* **2014**, *54*, 534; b) B. Russ, A. Glaudell, J. J. Urban, M. L. Chabinyc, R. A. Segalman, *Nat. Rev. Mater.* **2016**, *1*, 16050.
[5] H. Poleschner, W. John, F. Hoppe, E. Fanghänel, S. Roth, *J. Prakt. Chem.* **1983**, *325*, 957.
[6] a) Y. Sun, P. Sheng, C. Di, F. Jiao, W. Xu, D. Qiu, D. Zhu, *Adv. Mater.* **2012**, *24*, 932; b) Y. Sun, L. Qiu, L. Tang, H. Geng, H. Wang, F. Zhang, D. Huang, W. Xu, P. Yue, Y.-s. Guan, F. Jiao, Y. Sun, D. Tang, C.-a. Di, Y. Yi, D. Zhu, *Adv. Mater.* **2016**, *28*, 3351.
[7] a) F. Jiao, C.-a. Di, Y. Sun, P. Sheng, W. Xu, D. Zhu, *Philos. Trans. R. Soc., A* **2014**, *372*, 20130008; b) A. K. Menon, E. Uzunlar, R. M. W. Wolfe, J. R. Reynolds, S. R. Marder, S. K. Yee, *J. Appl. Polym. Sci.* **2017**, *134*; c) A. K. Menon, R. M. W. Wolfe, S. R. Marder, J. R. Reynolds, S. K. Yee, *Adv. Funct. Mater.* **2018**, *28*, 1801620; d) R. M. W. Wolfe, A. K. Menon, T. R. Fletcher, S. R. Marder, J. R. Reynolds, S. K. Yee, *Adv. Funct. Mater.* **2018**, *28*, 1803275; e) K. Wan, P. J. Taroni, Z. Liu, Y. Liu, Y. Tu, G. Santagiuliana, I.-C. Hsia, H. Zhang, O. Fenwick, S. Krause, M. Baxendale, B. C. Schroeder, E. Bilotti, *Adv. Electron. Mater.* **2019**, *5*, 1900582.
[8] L. Liu, Y. Sun, W. Li, J. Zhang, X. Huang, Z. Chen, Y. Sun, C. Di, W. Xu, D. Zhu, *Mater. Chem. Front.* **2017**, *1*, 2111.
[9] a) W. Shi, G. Wu, X. Yong, T. Deng, J.-S. Wang, J.-C. Zheng, J. Xu, M. B. Sullivan, S.-W. Yang, *ACS Appl. Mater. Interfaces* **2018**, *10*, 35306; b) X. Yong, W. Shi, G. Wu, S. S. Goh, S. Bai, J.-W. Xu, J.-S. Wang, S.-W. Yang, *J. Mater. Chem. A* **2018**, *6*, 19757.
[10] R. R. Schumaker, E. M. Engler, *J. Am. Chem. Soc.* **1977**, *99*, 5521.
[11] R. Tkachov, L. Stepien, R. Grafe, O. Guskova, A. Kiriy, F. Simon, H. Reith, K. Nielsch, G. Schierning, D. Kasinathan, C. Leyens, *Polym. Chem.* **2018**, *9*, 4543.
[12] R. Tkachov, L. Stepien, A. Roch, H. Komber, F. Hennersdorf, J. J. Weigand, I. Bauer, A. Kiriy, C. Leyens, *Tetrahedron* **2017**, *73*, 2250.
[13] R. Dong, M. Pfeffermann, H. Liang, Z. Zheng, X. Zhu, J. Zhang, X. Feng, *Angew. Chem., Int. Ed.* **2015**, *54*, 12058.
[14] a) A. P. Grosvenor, M. C. Biesinger, R. S. C. Smart, N. S. McIntyre, *Surf. Sci.* **2006**, *600*, 1771; b) R. Karthikeyan, D. Thangaraju, N. Prakash, Y. Hayakawa, *CrystEngComm* **2015**, *17*, 5431.
[15] M. Fantauzzi, B. Elsener, D. Atzei, A. Rigoldi, A. Rossi, *RSC Adv.* **2015**, *5*, 75953.
[16] a) H. B. Gray, E. Billig, *J. Am. Chem. Soc.* **1963**, *85*, 2019; b) S. I. Shupack, E. Billig, R. J. H. Clark, R. Williams, H. B. Gray, *J. Am. Chem. Soc.* **1964**, *86*, 4594; c) M. J. Baker-Hawkes, E. Billig, H. B. Gray, *J. Am. Chem. Soc.* **1966**, *88*, 4870.
[17] K. Ray, T. Weyhermüller, F. Neese, K. Wieghardt, *Inorg. Chem.* **2005**, *44*, 5345.
[18] R.-G. Xiong, B.-L. Song, X.-Z. You, T. C. W. Mak, Z.-Y. Zhou, *Polyhedron* **1996**, *15*, 991.
[19] M. T. S. De Mello, M. C. C. Ribeiro, P. S. Santos, *J. Raman Spectrosc.* **1995**, *26*, 173.
[20] P. J. Larkin, *Infrared and Raman Spectroscopy: Principles and Spectral Interpretation*, Elsevier, Waltham, MA **2017**.
[21] O. Bubnova, Z. U. Khan, H. Wang, S. Braun, D. R. Evans, M. Fabretto, P. Hojati-Talemi, D. Dagnelund, J.-B. Arlin, Y. H. Geerts, S. Desbief, D. W. Breiby, J. W. Andreasen, R. Lazzaroni, W. M. Chen, I. Zozoulenko, M. Fahlman, P. J. Murphy, M. Berggren, X. Crispin, *Nat. Mater.* **2014**, *13*, 190.
[22] S. Stoll, A. Schweiger, *J. Magn. Reson.* **2006**, *178*, 42.
[23] S. Remme, G. Lehmann, K. Recker, F. Wallrafen, *Z. Naturforsch. A* **1986**, *41*, 619.
[24] R. Stoyanova, E. Zhecheva, R. Alcántara, J. L. Tirado, *J. Phys. Chem. B* **2004**, *108*, 4053.
[25] N. S. Sariciftci, A. J. Heeger, Y. Cao, *Phys. Rev. B* **1994**, *49*, 5988.
[26] S. Sproules, K. Wieghardt, *Coord. Chem. Rev.* **2011**, *255*, 837.
[27] R. Matsuoka, R. Sakamoto, T. Kambe, K. Takada, T. Kusamoto, H. Nishihara, *Chem. Commun.* **2014**, *50*, 8137.
[28] a) R. Tsu, J. G. Hernandez, *Appl. Phys. Lett.* **1982**, *41*, 1016; b) D. Abol-Fotouh, B. Dörling, O. Zapata-Arteaga, X. Rodríguez-Martínez, A. Gómez, J. S. Reparaz, A. Laromaine, A. Roig, M. Campoy-Quiles, *Energy Environ. Sci.* **2019**, *12*, 716.